Turbulent Pipe Flow Subjected to a Mild Straining

Udhav U. Gawandalkar[1], Jerry Westerweel[1], Gerrit E. Elsinga[1,*]
1: Dept. of Mechanical, Maritime and Materials Engineering, Delft University of Technology, The Netherlands
* Correspondent author: g.e.elsinga@tudelft.nl

Keywords: Turbulence, Coherent Structures, Rapid Distortion

ABSTRACT

Turbulent pipe flow passing through a contraction is measured using planar PIV. The considered Reynolds numbers based on the pre-contraction pipe diameter are between Re_D = 12,300 and 47,900. The dimensionless strain rate imposed by the present contraction is restricted to 2.0, which means that the staining is rapid with respect to the integral time scale. When normalized with the Kolmogorov time scale, the strain is approximately unity at the center of the pipe. Therefore, the imposed strain is considered to be mild. It is found that the response of the streamwise velocity fluctuations (large scales) follow the predictions by Rapid Distortion Theory (RDT) within the experimental uncertainty. However, the radial velocity fluctuations, which are associated with smaller scales as compared to streamwise fluctuations, show a delayed response to the imposed strain. Such a delay is inconsistent with RDT. The present measurements, therefore, suggest a scale-depend response in agreement with some observations in other flows. The anomalous behavior of radial velocity fluctuations is discussed in relation to the coherent structures present in a turbulent pipe flow.

1. Introduction

The modelling of turbulence forced by an external straining is quite challenging. This is largely due to the different responses at large and small scales (Ayyalasomayajula & Warhaft 2006, Liu, Katz & Meneveau 1999). Moreover, an equilibrium between turbulence production and dissipation can no longer be assumed. When the imposed strain-rate is strong, that is, its associated time scale is short with respect to the eddy turn-over time, Rapid Distortion Theory (RDT) may apply (Hunt & Carruthers 1990). RDT basically assumes that the eddy has no time to adjust and that its vorticity is amplified passively according to the imposed strain. However, the shape of the energy spectrum predicted by RDT is inconsistent with observations (Ayyalasomayajula & Warhaft 2006). Even sophisticated turbulence modelling, i.e. Large Eddy Simulation (LES), yields unsatisfactory results due to the inability to accurately capture the scale-dependent responses (Liu, Katz & Meneveau 1999, Chen, Katz & Meneveau 2005). These results suggest that the response of (some) turbulent eddies is not passive, even if the strain is rapid, and that (fast) scale interactions remain important.

In order to examine these scale dependent responses and interactions, we consider the response of a turbulent pipe flow to the axisymmetric strain induced by a contraction. The streamwise and radial velocity components are measured inside the pipe and the contraction using planar PIV, which allows evaluating the turbulent kinetic energy (representing the larger scales) and spanwise vorticity (representing smaller scales). However, the present paper focuses on the velocity variances. It is shown that these variances reveal non-trivial (and scale dependent) behavior even though they are associated with large scales and are expected to follow RDT.

2. Experimental setup

The long pipe facility at the Laboratory for Aero & Hydrodynamics at Delft is employed with an axisymmetric contraction (figure 1). The pre-contraction length of $540D$ ensures that the incoming turbulent pipe flow is fully developed, where $D = 40$ mm is the pipe diameter. The length of the contraction is $L_c \approx D/2$ and the area-based contraction ratio is $C = 3$. We define the x and r axes along the streamwise and radial direction respectively, where the origin is located on the centerline at the start of the contraction. The corresponding components of the velocity fluctuations are given by u and v, whereas U and V indicate mean velocities. Furthermore, the coordinate $y = R(x) - r$ will be used to indicate the distance from the wall along the radial direction, where R is the local pipe radius.

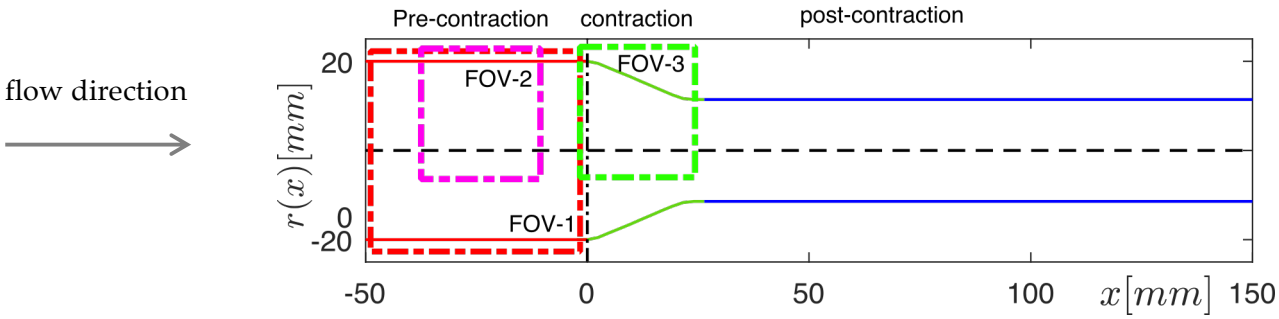

Fig. 1 A schematic diagram showing flow geometry in streamwise-radial (x-r) plane. The contraction is indicated by the thin green line, while the pre-contraction and post-contraction pipe sections are shown in red and blue respectively. Note that the edges of the contraction are rounded in order to prevent separation. The different fields of views (FOVs) used in the experiment are indicated by thick dash-dotted lines.

The contraction introduces an extensive straining in streamwise direction (x) and a compressive straining in the other directions. The idealized streamwise strain rate imposed on the turbulence is $S^* = \frac{(C-1)U_b}{L_c} \approx 2U_b/R_0$, where U_b is the bulk velocity velocity in the pipe upstream of the contraction and R_0 is the pipe radius upstream of the contraction. However, the effective local non-dimensional strain rate, $SR_0/U_b = \frac{dU}{dx}R_0/U_b$, is limited to approximately 1.9 along the centerline (see section 3). Furthermore, the induced strain rate is mildly rapid, meaning that its time-scale is faster than that of the large scales, but slower than the Kolmogorov time scale. The considered Reynolds numbers (Re_0) based on the incoming bulk velocity and pipe diameter are 12300, 28500, 37400 and 47900, as listed in table 1. Our lowest Reynolds number overlaps with the DNS of Jang, Sung & Krogstad (2011), though the present non-dimensional strain rate is slightly higher (1.9 compared to 1.3).

The flow velocity along the streamwise-radial (r-x) plane is measured using planar particle-image-velocimetry (PIV). The measurements were performed in three different field of views (FOV) (see figure 1). The velocity field in FOV-1 was used to verify that the incoming pipe flow is fully developed, while FOV-2 and FOV-3 are zoomed-in views to achieve the desired spatial resolution. The flow was seeded with tracer particles (Sphericell 110P8, Potter Industries) having a mean diameter of 12 μm and a nominal density of 1.1±0.5 g/cm^3. The r-x plane of the contraction was illuminated with a laser sheet which was ~70 mm wide and ~1 mm thick. The illumination source is a double-pulsed Nd:YAG laser (Quanta-Ray, Spectra-Physics), capable of producing energy of 400 mJ per pulse. The particle image recordings were acquired at 1.4 Hz using a high-resolution LaVision Imager Pro LX 16M camera (4872x3248 pixels, 12-bit, pixel pitch 7.4 μm) placed perpendicular to the light sheet. The camera was equipped with a 105 mm Micro-Nikkor objective lens set at $f/5.6$. This produced a geometric magnification of 0.49-0.90, depending on the FOV. The laser pulse separation (Δt) was set to restrict the maximum particle image displacement to 30 pixels (see table 2). Such a high displacement aids in resolving the turbulent statistics within the core of the pipe, where the turbulent velocity fluctuations are only a few percent of the bulk velocity. The raw particle images were then enhanced by performing background subtraction and min-max filtering. Finally, the velocity fields were evaluated using DaVis 8.4 with the final interrogation window size of 32×32 and 75% window overlap. Furthermore, the universal outlier detection (Westerweel & Scarano 2005) was used to remove the spurious vectors. The resulting in-plane spatial resolution is 0.27 mm based on the interrogation window size (IW) for FOV-2 and FOV-3, while the out-of-plane resolution is ~1 mm (laser sheet thickness). The former corresponds to approximately 2η–6.7η in the outer layer depending on the Reynolds number, where η is the Kolmogorov length scale. This means that the small scales are resolved when using 75%

interrogation window overlap (Tokgoz et al. 2012). The flow statistics were averaged over 6000 statistically independent snapshots. The measurement parameters are further listed in table 2.

Table 1 Properties of the turbulent pipe flow upstream of the contraction. The Kolmogorov length scale, η, is estimated using the theoretical expression $\eta^+ = (\kappa y^+)^{1/4}$ (Pope 2000, Stanislas et al. 2008), where κ is the Karman constant. Results are given for a wall-normal distance of $y^+ = 100$ and at the centerline, which are indicated by the subscripts 100 and c respectively. Here, the superscript + indicates a normalizing using the friction velocity, u_τ, and the kinematic viscosity, ν. The idealized imposed strain rate is $S^* = 2U_b/R$ for all cases. However, in Kolmogorov scaling, the imposed strain rate depends on the Reynolds number, which is shown in the last column.

Re_D	Re_τ	U_b (m/s)	u_τ (m/s)	ν (10^{-6} m^2/s)	η_{100} (mm)	η_c (mm)	$\tau_{\eta,100} = \eta_{100}^2/\nu$ (s)	$S^*\tau_{\eta,100}$
12,300	377	0.28	0.0174	0.923	0.1320	0.1870	0.0190	0.50
28,500	786	0.64	0.0356	0.905	0.0636	0.1077	0.0045	0.26
37,400	996	0.87	0.0461	0.926	0.0502	0.0903	0.0027	0.21
47,900	1238	1.15	0.0592	0.956	0.0404	0.0767	0.0017	0.18

Table 2 Specifications of the PIV settings.

FOV (#)	size FOV ($x \times y$) (mm^2)	IW (mm^2)	vector spacing (mm)	pulse separation, Δt (μs)			
				Re_D = 12,300	28,500	37,400	47,900
1	66×44	0.42×0.42	0.210	850	415	310	260
2	40×27	0.27×0.27	0.067	500	280	210	150
3	32×26.5	0.26×0.26	0.066	295	120	90	70

3. Results

The results presented in this section are for the case Re_D = 37400. Figure 2 shows the mean streamwise velocity at three different wall-normal positions, which are representative of the flow close to the wall ($y = 0.1R(x)$), at the approximate edge of the logarithmic layer ($y = 0.3R(x)$) and along the centerline. Just upstream of the contraction ($-1 < x/R_0 < 0$), the flow along the centerline is seen to accelerate slightly, while the flow close to the wall ($y = 0.1R$) decelerates slightly, such that the bulk velocity remains constant and mass conservation is satisfied. At $y = 0.3R$ the mean

streamwise velocity is approximately constant upstream of the contraction. These results signify that the flow already starts to adjust upstream of the contraction and that the radial profile of the mean velocity changes. This points to a general difficulty associated with rapid distortion as recognized before by Hussain & Ramjee (1976), who commented that 'even if a rapid distortion is provided, the flow will adjust itself so that the core flow corresponds to that of a smooth contraction'. A truly rapid distortion may thus be hard (or impossible) to achieve in practice and mild straining may potentially be more relevant. The latter assertion is further supported by the analysis of Kevlahan & Hunt (1997) who concluded that RDT fails immediately in the viscous range and increasingly so if the Reynolds number increases. This can also be inferred from the imposed strain rate normalized by the Kolmogorov time scale, which is given in the last column of table 1. However, RDT may still apply at larger scales, which will be examined below.

Inside the contraction ($0 < x/R_0 < 1$), a rapid acceleration of the flow is seen at all wall-normal positions as expected (figure 2). At the end of the contraction, the mean centerline velocity is increased by a factor 2.4, which is significantly lower than the 3-fold increase expected based on the contraction ratio (and hence the bulk velocity). However, this is compensated for by the flow close to the wall, which increases by a factor 3.7. Near $x/R_0 = 0.9$, the mean streamwise velocity is equal at the three wall-normal positions considered, which resembles plug flow locally. Finally, towards the end of the contraction, the mean streamwise velocity close to the wall exceeds the mean velocity near the centerline, which indicates a dramatic change in the radial velocity profile.

It is also evident from the mean velocity profiles that the noise level is increased inside the contraction as compared to the straight pipe. This is due to a lower optical quality of the model in that part, which mostly affects the streamwise velocity component. The radial component is much less affected, see below. In order to suppress the noise, a second order regression analysis was performed on the mean velocity profiles (black lines in figure 2). The second order polynomial was fitted over a streamwise distance of $0.39R$, which is acceptable given that the mean velocity is smooth.

Based on the regression, the mean streamwise acceleration, and hence the effective local non-dimensional strain rate, SR_0/U_b , can be estimated. Here the acceleration is taken equal to the local slope of the fitted polynomial. Along the centerline, the non-dimensional strain rate is at most 1.9 (figure 3), which is lower than the idealized imposed strain rate, $S^*R_0/U_b \approx 2$. This is consistent with the mean velocity increase along the centerline being lower than expected from the contraction ratio, as noted above. The strain rates at the other wall-normal positions are higher than along the

centerline (figure 3). Over the first half of the contraction the differences remain small. However, beyond $x/R_0 \approx 0.6$, some profound differences can be noticed. In particular, very high streamwise accelerations are found for $y = 0.1R$, which are related to the overshoot of the mean streamwise velocity close to the wall with respect to the centerline velocity.

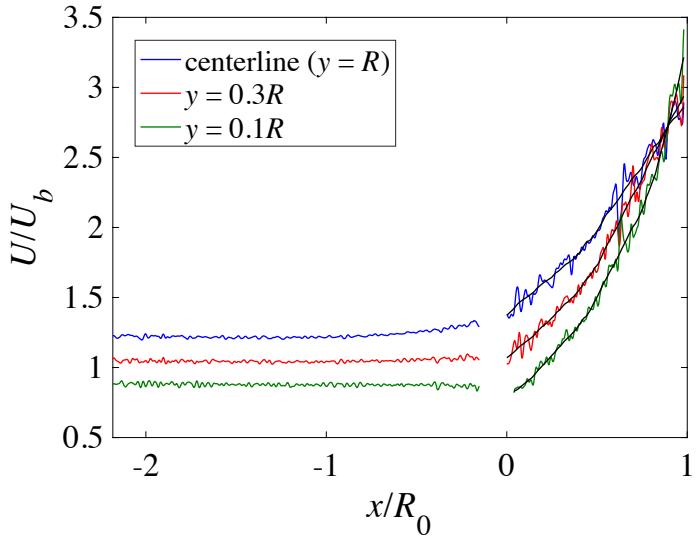

Fig. 2 Mean streamwise velocity at three different wall-normal distances y. The black lines show second order regressions of the velocity profiles inside the contraction.

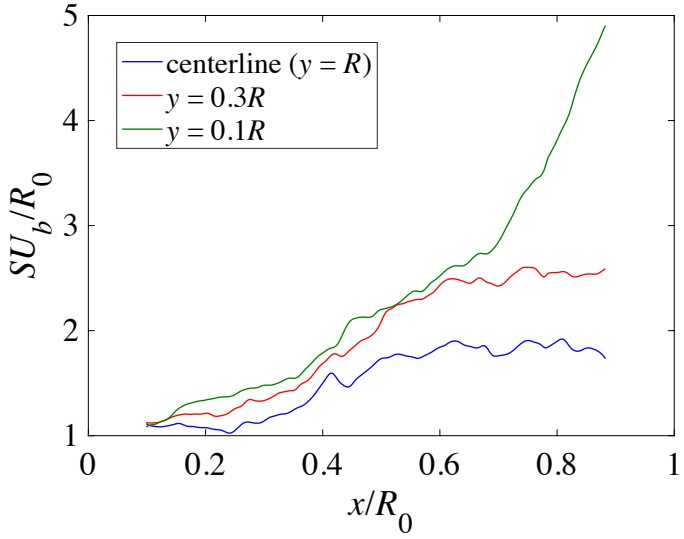

Fig. 3 Non-dimensional streamwise strain rates inside the contraction, which were obtained from the second order regressions shown in figure 2.

Having established the mean flow velocity and the effective strain rate, we turn the attention to the turbulent fluctuations. The fluctuations are quantified by means of the velocity variances, which are denoted by u^2 and v^2 for the streamwise and radial components respectively. (In our notation time-averaging symbols have been omitted for simplicity.) Variances can be biased by the contribution from measurement noise. In order to mitigate this effect, we considered the radial auto-correlations of u and v. Furthermore, the radial auto-correlation was averaged over a distance of $\pm 0.15R_0$ and $\pm 0.052R_0$ from the nominal position for the cases $y = R$ and $y = 0.3R$ respectively. The case $y = 0.1R$ is not considered here, because the data was too noisy. Assuming that noise remains correlated over at most two interrogation window sizes, and hence affects the correlation peak only up to that distance, we estimate the actual correlation peak (i.e. the actual variance) by fitting a parabola to the auto-correlation considering data points between 8 and 16 vector spacings away from the peak. Note that 16 vector spacings corresponds to approximately 12η at the centerline of the pipe, which is considered small compared to the correlation length for velocity fluctuations in a turbulent flow. Therefore, it is reasonable to assume that the points used in the fit belong to the actual correlation peak. A more elaborate discussion of this noise correction method can be found in Benedict & Gould (1998) and Romano et al. (1999). Based on this approach, the root-mean-square of the noise on an individual velocity component is estimated at 1.5–2.0% of U_b inside the straight pipe and 2.3–3.5% of U_b inside the contraction.

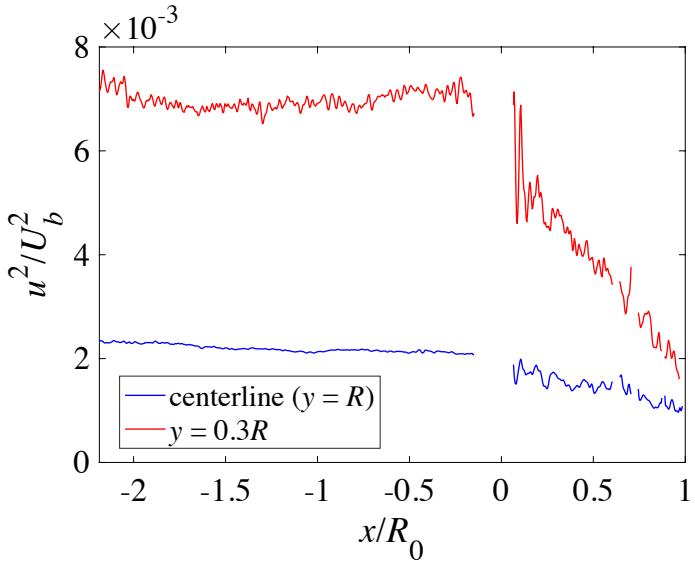

Fig. 4 Variance of the streamwise velocity fluctuations, u^2, at two different wall-normal distances y.

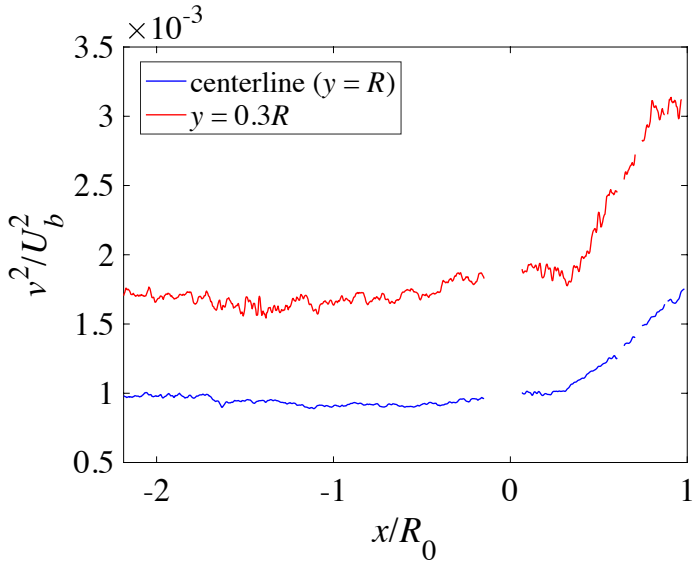

Fig. 5 Variance of the radial velocity fluctuations, v^2, at two different wall-normal distances y.

The noise corrected variances u^2 and v^2 are shown in figures 4 and 5. The streamwise variance decreases monotonically as expected from RDT. However, the radial variance reveals a more intricate behavior inside the contraction. Initially, up to $x/R_0 \approx 0.3$, the profiles in figure 5 are nearly flat, which suggests a delay in the response of the radial fluctuations of approximately $0.3R_0/U_b$ corresponding to 0.8 Kolmogorov time scales at the centerline. The scaling of the delay will have to be confirmed as the results from other Reynolds numbers become available. Following this initial delay, a rapid increase of the radial fluctuations is seen, as expected. Towards the end of the contraction, the radial variance is observed to level off for $y = 0.3R$, but not for the centerline.

Batchelor & Proudman (1954) have predicted the evolution of the variances in a symmetric contraction using RDT. Though, as commented by these authors, their assumption of homogenous turbulence (and homogenous imposed strain) and isotropy of the spectrum will not be valid in a pipe with a finite contraction, it still provides a valuable (and frequently used) reference and hence a qualitative comparison may be possible. Their prediction of u^2 and v^2 is given by (Batchelor & Proudman 1954):

$$\frac{u^2}{u_i^2} = \frac{3}{4}c^{-2}\left(\frac{1+\alpha^2}{2\alpha^3}\log\left(\frac{1+\alpha}{1-\alpha}\right) - \alpha^{-2}\right) \tag{1}$$

$$\frac{v^2}{v_i^2} = \frac{3}{4}c + \frac{3}{4}c^{-2}\left(\frac{1}{2}\alpha^{-2} - \frac{1-\alpha^2}{4\alpha^3}\log\left(\frac{1+\alpha}{1-\alpha}\right)\right) \tag{2}$$

where $c = U/U_i$, $\alpha^2 = 1 - c^{-3}$ and log is the natural logarithm. The subscript i refers to the initial value prior to the straining. These relations are conveniently compared with the measurement in a plot of the normalized variances versus $c = U/U_i$ (figures 6 and 7). Here, the initial conditions were taken in the straight pipe section at $x/R_0 \approx$ -0.25.

Along the centerline, the streamwise variance, u^2, is found to follow the RDT prediction within the experimental uncertainty as given by the high frequency oscillations in u^2 (figure 6). Closer to the wall at $y = 0.3R$, the measured streamwise variance, u^2, is slightly lower than the RDT prediction, but otherwise follows the expected trend. The plot for the radial variance, v^2, again highlights a delay in the response, during which v^2 is approximately constant (figure 7). The effect appears most pronounced at $y = 0.3R$. Furthermore, the subsequent increase in v^2 seems to be faster than predicted, i.e. the slope is steeper, along the centerline. However, the rate of increase at $y = 0.3R$ is comparable to the RDT prediction.

Therefore, it is concluded that the results for u^2 are close to expectations, but that some important deviations from RDT can be noted for v^2. In particular, the delayed response of v^2 is different from expectations. Some discussion on the origin of this delay is presented below.

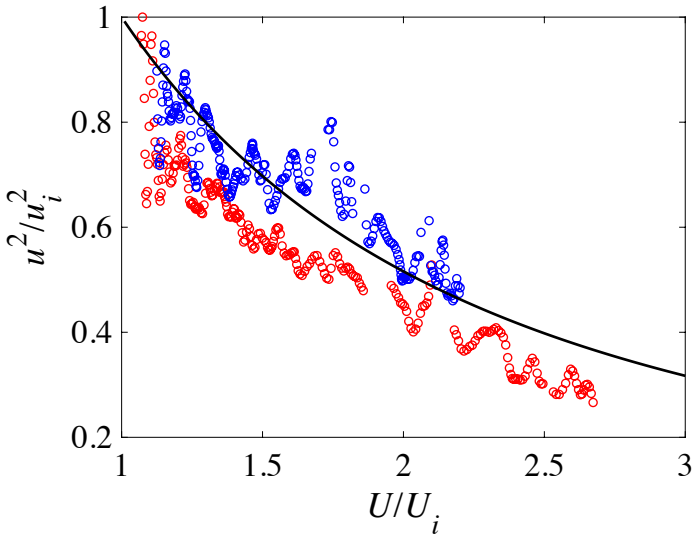

Fig. 6 Streamwise velocity variance, u^2, versus the local mean streamwise velocity, U, along the centerline (blue) and at $y = 0.3R$ (red). Note that U has been filtered using the second order regression (see figure 2). The RDT prediction (equation (1)) is given by the black line.

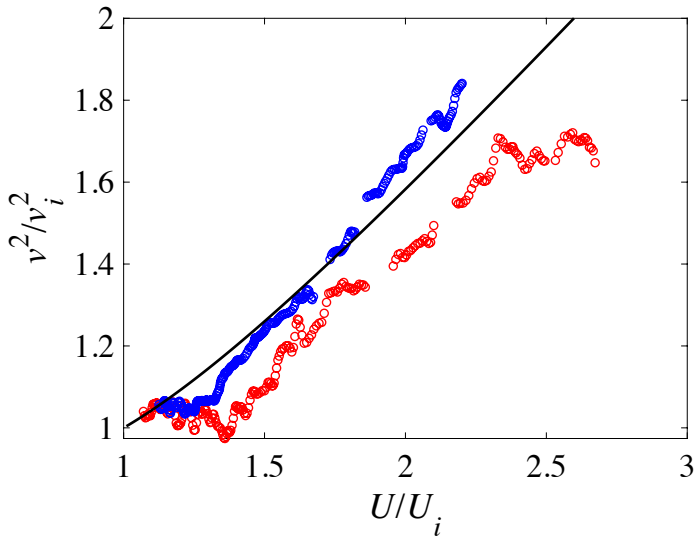

Fig. 7 Radial velocity variance, v^2, versus the local mean streamwise velocity, U, along the centerline (blue) and at $y = 0.3R$ (red). Note that U has been filtered using the second order regression (see figure 2). The RDT prediction (equation (2)) is given by the black line.

4. Discussion

The delayed response of v^2 is interesting, because it is precisely these scale-dependent delays that are poorly understood and pose a challenge when modelling turbulence forced by an external straining (Ayyalasomayajula & Warhaft 2006, Liu, Katz & Meneveau 1999), as mentioned already in the introduction. Although we had initially expected such delays to appear only for the smallest scales (e.g. the vortices), wall-normal velocity does represent a smaller scale than streamwise velocity, that is, the peak contributions to the energy spectra of u are at larger wavelengths as compared to v (e.g. Elsinga et al. 2010). However, v does not represent the smallest (dissipative) scale.

The advantage of considering wall-bounded turbulence is that the flow structures have been extensively studied and documented, see Adrian (2007) for a review. Furthermore, the large scales are strongly aligned with the streamwise direction, as compared to having random orientations in homogeneous isotropic, which simplifies the problem. This allows us to speculate on the origin of the observed delay and the possible implications for the smallest scales.

A simplified structural description of canonical wall-bounded turbulence is as follows. Within the outer layer, the u-component of velocity is associated with so-called very-large scale motions (VLSMs). These VLSMs are elongated high and low speed regions with an associated streamwise wave length between and 8R and 20R and they contain approximately half the turbulent kinetic energy of the streamwise component (Guala, Hommema & Adrian 2006). Similar VLSMs are also seen in turbulent boundary layers and channel flows. Alongside these very-long high and low speed regions, streamwise vortices develop with a characteristic length of ~1R (Elsinga et al. 2010), which induce a secondary flow in the radial and azimuthal direction. This is consistent with the streamwise velocity fluctuations being associated with larger scales as compared to radial/wall-normal velocity fluctuations. Furthermore, the induced secondary spanwise flow imposes a stretching motion on the small-scale spanwise vorticity, which is organized in shear layers located above the large-scale low speed regions (Gul, Elsinga & Westerweel 2020). This spanwise stretching is important because it causes these layers to remain thin and the spanwise vorticity magnitude to remain significant.

In the above structural description, spanwise fluctuations are linked to the wall-normal fluctuations, because they are induced by the same large-scale streamwise vortices. This suggests that a delay in the response of v is accompanied by a delayed response of the spanwise velocity, and hence the spanwise straining imposed on the small-scale spanwise vorticity. This implies a delayed response of the small-scale spanwise vorticity, which will need to be confirmed in a further analysis of the data. The above further suggests that the understanding of the v^2 delay is critical.

We hypothesize that the v^2 delay could be a pressure effect. The leading terms in the Reynolds stress transport equation for v^2 are the production term and the pressure term. It seems implausible that viscous effects play a role in the observed delay, since that would imply that the small (dissipative) scales respond faster than the larger scale v motions. Furthermore, our data suggests that the transport terms are negligible in the core of the contraction. Neglecting transport and viscous terms leads to the following reduced evolution equation for v^2:

$$\frac{Dv^2}{Dt} \approx -2v^2\frac{\partial V}{\partial r} - 2v\frac{\partial p}{\partial r} \tag{3}$$

The velocity gradient $\frac{\partial V}{\partial r}$ is negative (compression), which means that the first term on the right-hand side (the production term) is positive inside the contraction. The second term on the right-hand side, i.e. the pressure term, contains the correlation between the radial velocity fluctuations

and the fluctuating pressure gradient in the radial direction. During the delay, v^2 is approximately constant, which means that the material derivative in equation (3) is close to zero and that the production term is balanced by the pressure term. The latter, therefore, needs to be negative, and hence $\frac{\partial p}{\partial r}$ is positively correlated with v. This can be understood by considering a positive radial velocity fluctuation ($v > 0$) near the wall (say at $r = 0.7R$ corresponding to $y = 0.3R$), which enters the contraction from the straight pipe. In that case the flow is directed towards the wall, whereas the wall is now 'moving' in the opposite direction as perceived by the fluid due to the contraction. This suddenly leads to a stronger blocking of the wall and a stronger opposing force/pressure gradient relative to the mean, i.e. an increased local pressure gradient in the radial direction ($\frac{\partial p}{\partial r} > 0$). The result is a positive contribution to the correlation $v\frac{\partial p}{\partial r}$. On the other hand, a negative radial velocity fluctuation entering the contraction is compatible with the boundary condition, which may relieve the local pressure gradient ($\frac{\partial p}{\partial r} < 0$) such that the product of the local radial velocity fluctuation and the pressure gradient is again positive. In that case both negative and positive v contribute to a positive correlation $v\frac{\partial p}{\partial r}$. Note that this explains the sign of the pressure term, but not yet its magnitude. The latter remains an open issue.

The above could be considered as an inlet effect associated with a sudden change in the strain where the velocity needs time to respond to a new boundary condition in the wall-normal direction (inertia). We further note that the pressure term switches sign in the core, from positive inside the straight pipe section to negative inside the contraction (Jang, Sung & Krogstad 2011). The latter is consistent with the negative contribution inferred above. However, the delayed response of v^2 is not immediately evident in their results, which could be explained by the gradual contraction inlet in their case. Moreover, previous hotwire measurements were taken with a relatively coarse streamwise resolution, which may have been insufficient to resolve a possible delay.

5. Conclusions

Turbulent pipe flow passing through a contraction has been measured at high spatial resolution using planar PIV. The strain rate imposed by the contraction was rapid with respect to the largest scales in the flow. However, the imposed strain rate was increasingly slow with respect to the dissipative scales as the Reynolds number increased. This demonstrates that a true rapid distortion at all scales is difficult (or even impossible) to achieve in practice, which is consistent with ideas expressed in the literature (Hussain & Ramjee 1976, Kevlahan & Hunt 1997). Inside the contraction, the evolution of u^2 was close to expectations. However, some important deviations from RDT were

noted for v^2. In particular, the delayed response of v^2 was different from predictions, which was explained as a pressure effect in the contraction inlet.

References

Adrian, R. J. (2007). Hairpin vortex organization in wall turbulence. *Physics of fluids*, 19(4), 041301

Ayyalasomayajula, S. & Warhaft, Z. (2006). Nonlinear interactions in strained axisymmetric high-Reynolds-number turbulence. *Journal of Fluid Mechanics,* 566: 273-307.

Batchelor, G. K., & Proudman, I. (1954). The effect of rapid distortion of a fluid in turbulent motion. *The Quarterly Journal of Mechanics and Applied Mathematics*, 7(1), 83-103.

Benedict, L. H., & Gould, R. D. (1998). Concerning time and length scale estimates made from burst-mode LDA autocorrelation measurements. *Experiments in fluids*, 24(3), 246-253.

Chen, J., Katz, J. & Meneveau, C. (2005). Implication of mismatch between stress and strain-rate in turbulence subjected to rapid straining and destraining on dynamic LES models. *J. Fluids Engin.* 127: 840-850.

Elsinga, G. E., Adrian, R. J., Van Oudheusden, B. W., & Scarano, F. (2010). Three-dimensional vortex organization in a high-Reynolds-number supersonic turbulent boundary layer. *Journal of Fluid Mechanics*, 644, 35-60.

Guala, M., Hommema, S. E., & Adrian, R. J. (2006). Large-scale and very-large-scale motions in turbulent pipe flow. *Journal of Fluid Mechanics*, 554, 521-542.

Gul, M., Elsinga, G. E., & Westerweel, J. (2020). Internal shear layers and edges of uniform momentum zones in a turbulent pipe flow. *Journal of Fluid Mechanics*, 901. A10

Hunt, J.C. & Carruthers, D.J. (1990). Rapid distortion theory and the 'problems' of turbulence. *Journal of Fluid Mechanics,* 212: 497-532.

Hussain, A.K.M.F. & Ramjee, V. (1976). Effects of the axisymmetric contraction shape on incompressible turbulent flow. *J. Fluids Engin.* 98, 58-68.

Jang, S. J., Sung, H. J., & Krogstad, P. Å. (2011). Effects of an axisymmetric contraction on a turbulent pipe flow. *Journal of fluid mechanics*, 687, 376-403.

Kevlahan, N. R., & Hunt, J. C. R. (1997). Nonlinear interactions in turbulence with strong irrotational straining. *Journal of Fluid Mechanics*, 337, 333-364.

Liu, S., Katz, J. & Meneveau, C. (1999). Evolution and modelling of subgrid scales during rapid straining of turbulence. *Journal of Fluid Mechanics,* 387: 281-320.

Pope, S. B. (2000). *Turbulent flows*. Cambridge University Press.

Romano, G. P., Antonia, R. A., & Zhou, T. (1999). Evaluation of LDA temporal and spatial velocity structure functions in a low Reynolds number turbulent channel flow. *Experiments in fluids*, 27(4), 368-377.

Stanislas, M., Perret, L., & Foucaut, J. M. (2008). Vortical structures in the turbulent boundary layer: a possible route to a universal representation. *Journal of Fluid Mechanics*, 602, 327-382.

Tokgoz, S., Elsinga, G. E., Delfos, R., & Westerweel, J. (2012). Spatial resolution and dissipation rate estimation in Taylor--Couette flow for tomographic PIV. *Experiments in fluids*, *53*(3), 561-583.

Westerweel, J., & Scarano, F. (2005). Universal outlier detection for PIV data. *Experiments in fluids*, *39*(6), 1096-1100.